Visible quasi-phasematched harmonic generation by electric-field-poled lithium niobate

G. D. Miller, R. G. Batchko, M. M. Fejer, and R. L. Byer

Ginzton Laboratory, Stanford University, Stanford, CA 94305
gdmiller@loki.stanford.edu

ABSTRACT

Laser-based displays and illumination systems are applications which can capitalize on the brightness and efficiency of semiconductor lasers, provided that there is a means for converting their output into the visible spectrum. Semiconductor laser manufacturers can adjust their processes to achieve desired wavelengths in several near-infrared bands; an equally agile conversion technology is needed to permit display and illumination system manufacturers to choose visible wavelengths appropriate to their products. Quasi-phasematched second harmonic generation has the potential to convert high-power semiconductor laser output to the visible with 50% optical-to-optical conversion efficiency in a single-pass bulk configuration, using electric-field-poled lithium niobate. Lithographically-defined electrode structures on the positive or negative polar faces of this crystal are used to control the formation of domains under the influence of electric fields applied using those electrode structures. The quality of the resulting domain patterns not only controls the efficiency of quasi-phasematched second harmonic generation, but also controls the degree of resistance to photorefractive damage. We present a model which is used to identify the optimum electrode duty cycle and applied poling field for domain patterning and compare the predicted domain duty cycle with experimental results. We discuss factors which contribute to inhomogeneous domain pattern quality for samples poled under otherwise ideal conditions and our progress in limiting their influence. Finally, we present optical characterization of a 2.4 mm long 500 μm thick sample which produced an average second harmonic power of 1.3 W of 532 nm green from a 9 W average power Q-switched 1064 nm Nd:YAG laser in a loose-focus single-pass configuration.

Keywords: nonlinear optics; quasi-phasematching; second harmonic generation; lithium niobate; electric field poling; ferroelectric domains; periodic poling.

1. INTRODUCTION

1.1 The potential for quasi-phasematched non-linear optics in visible light generation

With a nonlinearity of 27 pm/V, first-order quasi-phasematched (QPM) lithium niobate can produce 430 nm blue light from an 860 nm laser focused through the crystal, with a normalized efficiency of 7.5 %/W-cm. Ideally, a device 3.2 cm long and driven by a 2 watt laser would have a 50% optical-to-optical conversion efficiency. This device would require a periodic domain structure with a 3.125 μm period for operation at 39°C, and temperature control to within 0.1°C[1]. (Alternatively, the laser's output wavelength can be made to track the phasematching wavelength of the sample over the desired temperature range). Given the trends in semiconductor laser technology, it is not unreasonable to anticipate the availability of suitable laser sources in the near future. With a spot size on the entrance face of the doubler of 62 μm, devices with a 0.25 mm by 0.25 mm aperture would permit fairly relaxed package alignment tolerances. A blue source of this description could find use in an 800 lumen desktop computer display having a wall plug efficiency of nearly 20% and an overall luminous efficiency in excess of 100 lm/W. Clearly, the successful development of high quality domain-patterned lithium niobate is likely to have a significant impact in applications requiring high power visible light sources.

When considering domain pattern quality, there are two main issues: periodicity and duty cycle. Domain periodicity has a strong effect on the phasematching wavelength of a QPM device. Considering a linear taper in periodicity as a first-order periodicity error, we find that taper must be kept below $1.7\,(\Lambda/L)^2$, where Λ is the average domain period and L is the device length[1]. For a 3.2 cm long device with a 3.125 μm period, the taper must be less than 17 nm/m. For lithographically-defined electrode patterns, this condition is easily satisfied. However, the inhomogeneity in substrate dispersion must also be kept within this limit. Fortunately, materials such as lithium niobate, which are fabricated in high volume with a well-established technology, can easily satisfy this requirement.

Domain pattern duty cycle quality affects both peak device efficiency and resistance to photorefractive damage. Maximum conversion efficiency is achieved for a perfectly uniform 50% domain duty cycle. In order to realize at least half of the

 0-8194-2074-3/96/$6.00

maximum possible efficiency, a sample's mean duty cycle must be kept within 25% of ideal, rms duty cycle variation must be kept below 17%, and no more than 14% of the interaction length can be lost to missing or run-together domains.[1] Photorefractive damage resistance in bulk devices is influenced most strongly by duty cycle averaged over dimensions on the order of the beam diameter and imposes a more stringent limitation on duty cycle quality than efficiency considerations alone.[2] While lithographically-defined electrode duty cycle and applied poling field have a significant effect on the resulting domain pattern duty cycle, variations within the substrate can create clusters of lowered domain pattern quality, as we will show in this paper. Consequently, reproducible domain patterning for visible light generation will involve not only control over lithographic and poling processes, but must also encompass substrate preparation processes as well.

1.2 Organization of this paper

In Section 2, we provide a brief review of the progress-to-date in visible second harmonic generation (SHG) with electric-field domain-patterned ferroelectrics and present a generic view of the process itself. In Section 3, we present an electrostatic model which is used to identify the optimum electrode duty cycle and applied poling field for domain patterning, and compare with experimental results. In Section 4, we discuss factors which contribute to inhomogeneous domain pattern quality for samples poled under otherwise ideal conditions and our progress in limiting their influence. In Section 5, we present optical characterization of a 2.4 mm long 500 μm thick sample which produced an average power of 1.3 W of 532 nm green from a 9 W average power Q-switched 1064 nm Nd:YAG laser in a loose-focus single-pass configuration. In Section 6 we provide a summary of this work and discuss the next priorities for attaining repeatable domain patterning for visible SHG devices.

2. ELECTRIC FIELD DOMAIN PATTERNING BACKGROUND AND PERSPECTIVE

2.1 Progress in visible SHG

The use of electric fields applied by means of periodic electrodes on one of the polar faces of lithium niobate to pattern its domain structure was first demonstrated by Yamada, et. al., in 1993[3]. In their report, 20.7 mW of 426 nm blue light was generated in a waveguide with a 2.8 μm domain period from a 196 mW Ti:Al_2O_3 laser. Although the waveguide was 3 mm long, the interaction length for second harmonic generation was 1 mm. Since that time, a number of authors have reported progress in applying the technique principally to lithium niobate[4], lithium tantalate[5], and KTP[6]. Electric field domain-patterned substrates are being used in sum-frequency[7], difference-frequency, and optical parametric oscillator[8] applications in addition to quasi-phasematched second harmonic generation applications..

It is evident from the literature that, while domain periods greater than 20 μm in lithium niobate can be repeatably obtained over full wafers, difficulties arise for the shorter periods (3 -7 μm) required for visible first-order quasi-phasematched second harmonic generation in this material. These difficulties are characterized by sample-to-sample variations in pattern quality. For sufficiently short samples, pattern quality can be nearly ideal: Recent work[9] has shown that excellent pattern quality is achievable for 4.6 μm gratings over an interaction length of 6 mm using 200 μm thick samples. In this experiment, 49 mW of 473 nm blue light was generated internal to the sample from 1.07 W of 946 nm fundamental light in a single-pass configuration. Not only are domain period and sample size important influences on pattern quality, but sample thickness also plays a significant role. These same workers found that pattern quality was reduced in thicker substrates (300 μm), even for longer grating periods (6.4 μm) and shorter sample lengths (3.2 mm).[10] Despite these difficulties, they were able to generate an average power of 275 mW of 523.5 nm green from a 650 mW CW mode-locked 1047 nm laser.

To understand the nature of these difficulties, we begin with a description of a prototypical electric field domain-patterning configuration and then partition the domain formation process into four distinct regimes.

2.2 Prototypical poling configuration

Figure 1 below shows a prototypical poling configuration for patterning the domain structure of ferroelectrics. The sample is shown here to have a lithographically-defined periodic electrode structure on its +Z face. The electrodes are then overcoated with an insulator and contacted at their ends with an electrolyte. The -Z face is contacted uniformly with electrolyte. The sample is clamped between a pair of o-rings to prevent arcing and connected to the high voltage signal generator by means of electrodes which contact the electrolyte inside the fixture. The source impedance varies widely among experimenters, but is set to zero for this report. The vertical stripes under the electrodes represent domain-reversed

material, also indicated with downward-pointing arrows. The arrows point in the direction of the local spontaneous polarization. The striped regions in the substrate are shown to have spread in width beyond the width of the electrodes. The nature of this spreading is discussed in Section 3.

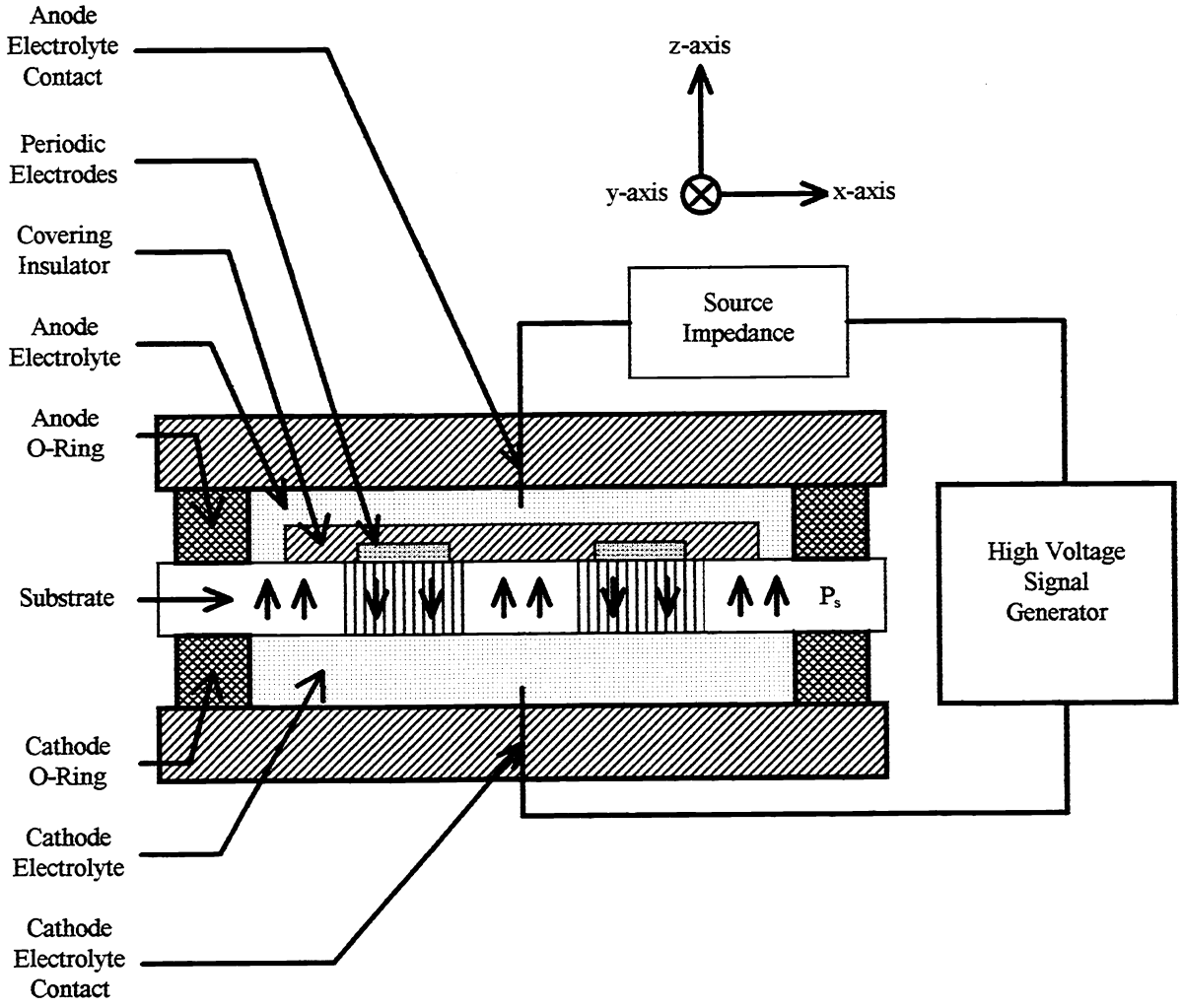

Figure 1. Prototypical Poling Configuration

2.3 Four distinct regimes of domain formation

Domain formation can be broken into four distinct regimes: nucleation, tip propagation, wall propagation, and stabilization. We will briefly discuss each regime and then turn to a more detailed discussion of wall propagation since this regime determines the final width of domains.

2.3.1 The nucleation regime

In a single domain crystal, the nucleation regime occurs as the electric fields within the crystal are raised above a threshold value, commonly referred to as the coercive field, E_c. In lithium niobate, this coercive field is approximately 20.5 kV/mm. At or above the coercive field, microscopic domains form, typically at the +Z and -Z faces of the sample. We have also observed the nucleation of domains within the volume of the crystal. The observation of volume nucleation is an especially strong indicator of substrate inhomogeneity, since it is energetically unfavorable for domains to nucleate in the volume of a homogeneous crystal.

2.3.2 The tip propagation regime

The tips of the nucleated domains then propagate rapidly toward the faces of the crystal in the tip propagation regime. As the tips propagate, the domain walls spread outward in the x-y plane, widening the domains. While the ratio of tip velocity to wall velocity is difficult to measure, we find that its value lies between 100:1 and 1000:1 for lithium niobate. Usually, domains nucleated within a micron of one another can propagate through a 500 μm thick substrate without merging together. We have also observed cases where domain tips bend abruptly toward or apart from one another as they propagate through the crystal, as though some local inhomogeneity was distorting their trajectories. Often, these distorted trajectories are associated with the merging of domain tips as they propagate through the crystal.

2.3.3 The wall propagation regime

When the domain tips reach the polar faces of the crystal, the domain walls straighten to become nearly parallel to the polar axis, and the domain enters the wall propagation regime. Here, the domain walls move in the x-y plane with a velocity determined primarily by the applied electric field. By taking measures to first ensure preferential nucleation at the lithographically defined electrodes, and second to minimize the merging of domain tips through substrate pre-selection or special preparation techniques, the wall propagation regime controls the resulting domain duty cycle, and so is the subject of Section 3.

2.3.4 The domain stabilization regime

Attempts to control the resulting domain duty cycle by rapidly setting the applied field to zero will cause a phenomenon we call "flip-back", where all the domains initially formed will revert to their original unpatterned state. Flip-back implies the presence of a built-in field associated with domain formation. This built-in field has a decay constant on the order of 60 ms in lithium niobate, meaning that by lowering the field to zero in a time longer than 60 ms the domains will become stable. The stabilization regime appears to be a local phenomenon in the material, since we have observed that when forming large single domains and then permitting flip-back, the earliest formed parts of the domain would typically not flip back, if they had been under at least 18 kV/mm for greater than 60 ms.

3. AN ELECTROSTATIC MODEL OF THE ELECTRIC FIELD DOMAIN PATTERNING PROCESS

In this Section, we present a model of the electric field domain patterning process centered around the dynamics of the wall propagation regime. This regime is chosen as the starting point for a more complete model since it is in this regime that the majority of poling charge is delivered to the sample, and, in turn, the majority of the domain pattern is formed. An electrostatics-based approach was chosen since the time scales of domain patterning were much slower than any field settling times except for those associated with the stabilization regime. The stabilization regime does not appear at this point to have played a significant role in controlling the formation or interaction of domains. We also assume that both the substrate and insulator can be treated as ideal dielectrics. We point out that the role of strain in domain formation has been assumed to be of second order in lithium niobate since we have not yet been able to affect domain growth by varying strain conditions in the sample.

Perhaps the most significant assumption in this model is that domain wall velocity is governed primarily by the average field in the substrate. This assumption is derived from our observations that domain walls most commonly are observed to be parallel to the polar axis, nearly independent of surface features. In addition, the ratio $P_s/(\varepsilon E_c)$ sets the minimum long-range domain wall slope at 150:1, where $P_s = 0.78$ C/m^2 is the spontaneous polarization, $\varepsilon = 248$ pF/m is the permittivity of the crystal, and $E_c = 20.5$ kV/mm is the field required to cause domain reversal in the time scale under consideration. A domain wall with a shallower slope would produce fields high enough to cause domain reversals that in turn would increase the domain wall slope, bringing it more nearly parallel to the polar axis.

In Section 3.1, we show that there is a calculable electrostatic relationship between the amount a periodic domain pattern has spread underneath the insulator and the resulting average substrate field. In Section 3.2, data and a curve fit are presented that relates the velocity of domain walls to average substrate field and we identify the field at which domain wall velocity is most sensitive to changes in average substrate field. In Section 3.3, the electrostatic calculations and domain wall velocity fit are combined to predict electrode widths expected to result in a 50% domain duty cycle. In Section 3.4, the electrostatic calculations, velocity-field relationship, and poling field and electrode width optimizations are combined to predict poling current, which is then compared to the actual poling current of a sample poled under near-optimal

conditions. Finally, in Section 3.5, the resulting domain pattern quality of a sample poled under near-optimal conditions is analyzed.

3.1 Average substrate field vs. domain duty cycle

In a periodic electrode structure, as domains spread beyond the edges of the electrodes, they deposit spontaneous polarization charge on the interface between the insulator and substrate. This bound spontaneous polarization charge acts to lower the average substrate field. In Figure 2 below, we show the results of a calculation of average substrate field as a function of domain duty cycle for a 500 μm thick substrate with 0.5 μm thick spin-on-glass over a periodic electrode structure with a 6.5 μm period and 2.7 μm electrode width. Note that the average substrate field is unchanged until the domains have reached a duty cycle equal to the electrode duty cycle. Then, as the domains continue to grow in width, the average substrate field monotonically decreases.

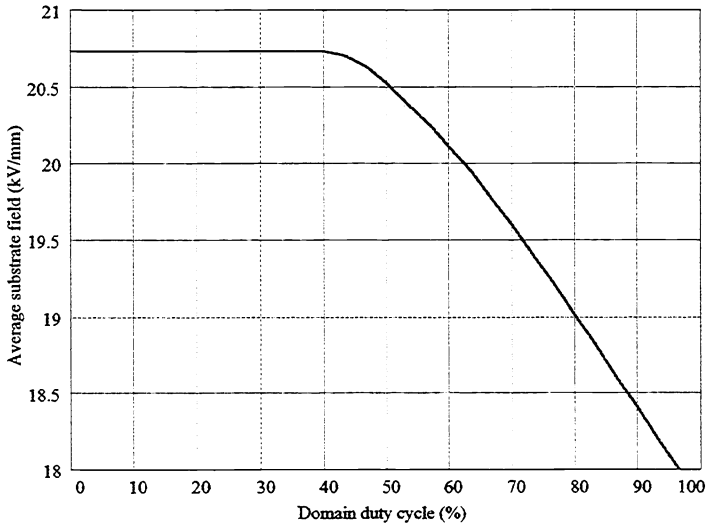

Figure 2. Average substrate field vs. domain duty cycle for 500 μm thick substrate with 0.5 μm thick spin-on-glass insulator, 2.7 μm wide electrodes on 6.5 μm period.

3.2 Domain wall velocity vs. electric field

To measure domain wall velocity as a function of applied field, 500 μm thick samples with no electrodes or insulator on the surface were poled for times sufficient to grow domains nominally 10 μm in diameter at fields ranging from 19.5 kV/mm to 27.25 kV/mm. A control set was also poled for times sufficient to grow domains 20 μm in diameter to verify the hypothesis that domain wall velocity was constant for a constant applied field. A 10 μm domain diameter was chosen in order to obtain a significant number of isolated domains, since we observed that domains adjacent to one another can merge with rapid wall movement. Each sample was then etched for five minutes in room temperature hydrofluoric acid to reveal the hexagonal domains. Using a calibrated microscope eyepiece graticle, the facet-to-facet diameter was measured for several of the largest isolated perfectly hexagonal domains on each sample. The diameters were divided by two to obtain the domain radii and then divided by the pulse duration to obtain domain wall velocity. The computed velocities are plotted in Figure 3 below as a function of applied field..

We examined the samples for distorted hexagons to rule out the possibility of domain wall velocity inhomogeneity. We found that nucleation tended to occur in clusters, and that within each cluster there were both large and small domains. Within these clusters the hexagons were undistorted, aside from instances where it appeared that pairs of domains merged into one. The absence of distorted hexagons established that domain wall velocity was uniform on the spatial scale of several hundred microns. Because poling times were extremely long at the low field conditions (3 hr at 19.5 kV/mm), we found that we could avoid breakdown by using lithium chloride dissolved in isopropanol as an effective electrolyte. At high fields, the pulse duration of 15 μs required a more conductive electrolyte, lithium chloride in deionized water. Between

21 kV/mm and 23.5 kV/mm, samples were poled with each electrolyte to assess the possible influence of the choice of electrolyte. In this range of fields, the choice of electrolyte had no significant influence.

The largest domains observed at each field were selected for curve fitting, since we observed that the number of domain nuclei per unit area was both a function of applied field and pulse duration, especially at fields below 22.5 kV/mm. The largest domains were assumed to be the earliest nucleators and thus the best estimators of the domain velocity. We found a satisfactory fit to our data by allowing for the possibility of a pair of threshold-activated processes controlling domain wall velocity. Using a functional form motivated by the results of Hayashi[11], our fit is given in the equation below, where v(E) is domain wall velocity as a function of applied field.

$$v(E) = \Phi(E - E_1)\, v_1\, e^{-\frac{\delta_1}{\frac{E}{E_1}-1}} + \Phi(E - E_2)\, v_2\, e^{-\frac{\delta_2}{\frac{E}{E_2}-1}}$$

where Φ is the Heaviside step function, E_1=19.4 kV/mm, v_1=16.3 m/s, δ_1=1.29, E_2=15.0 kV/mm, v_2=362 μm/s, and δ_2=3.83. This curve fit is plotted along with the experimental data in Figure 3.

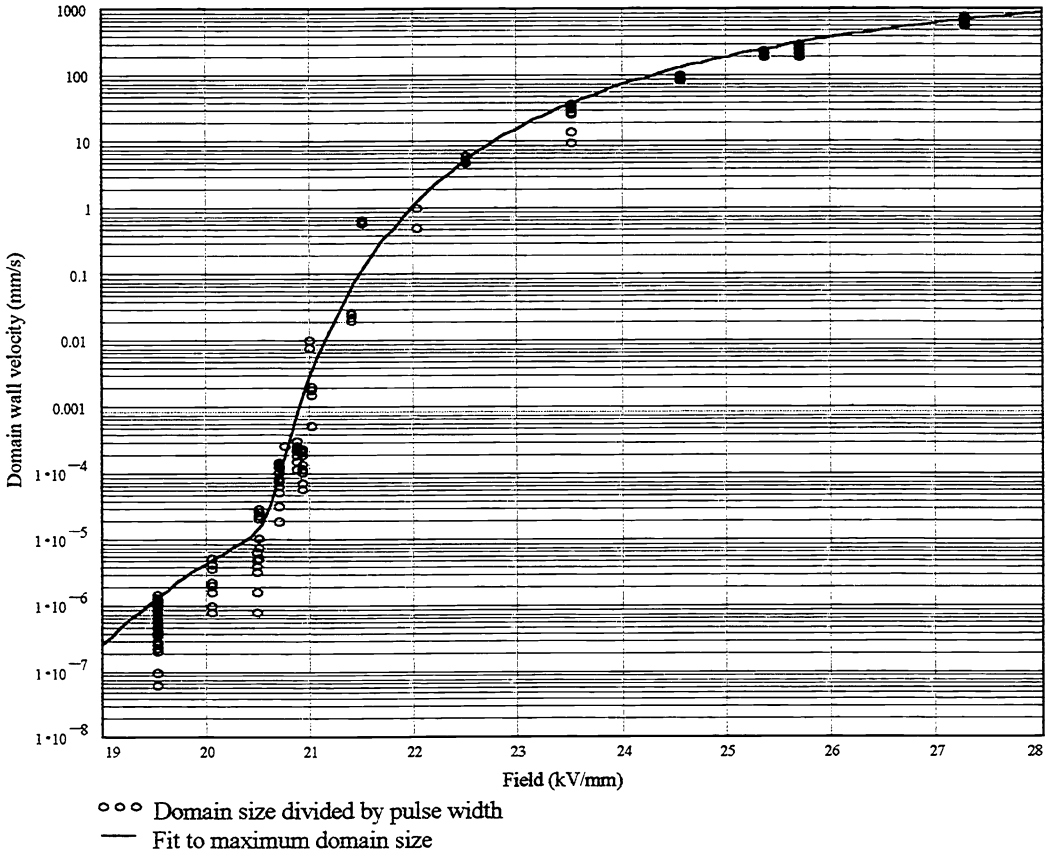

Figure 3. Domain wall velocity vs. applied field.

In Figure 4, we plot the contrast of the domain patterning process, defined as the logarithmic derivative of velocity, as a function of average substrate field. From this plot, we see that the maximum process contrast occurs at an applied field of 20.75 kV/mm. Domain spreading is most strongly inhibited by the spontaneous polarization charge deposited at the insulator-substrate interface when poling lithium niobate at this field.

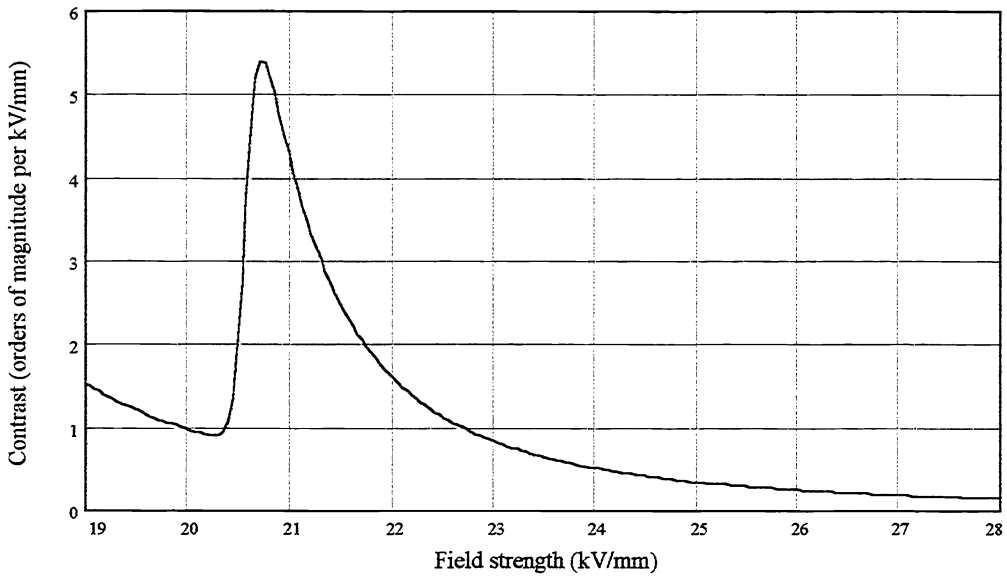

Figure 4. Process contrast as a function of applied field.

3.3 Predicted optimum electrode widths

By combining the electrostatic model with the field-dependent domain wall velocity function, we have generated a plot of electrode widths which are predicted to yield a nominal 50% domain duty cycle for domain periods from 1 μm to 100 μm, for 500 μm thick substrates with 0.5 μm thick spin-on-glass overcoat, poled at 20.75 kV/mm in Figure 5 below.

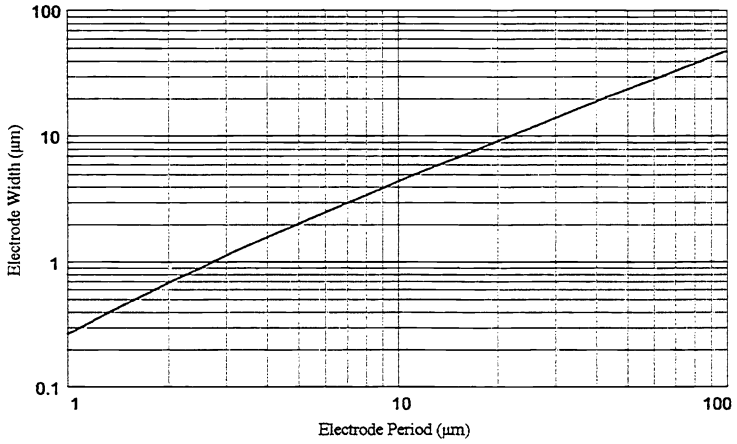

Figure 5. Predicted optimum electrode width as a function of electrode period for 500 μm thick samples overcoated with 0.5 μm thick spin-on-glass insulator.

3.4 Time-dependent poling current

By combining the electrostatic model with the field-dependent domain wall velocity function, we computed poling current vs. time and compared it with the current trace of a sample poled under near-optimal conditions (see Figures 6a and 6b). We find that the domain patterning process is essentially self-terminating both in theory and in practice, meaning that application of pulses longer than those required to complete patterning will have little effect on the resulting domain duty cycle, as long as the samples are poled at the maximum contrast poling field.

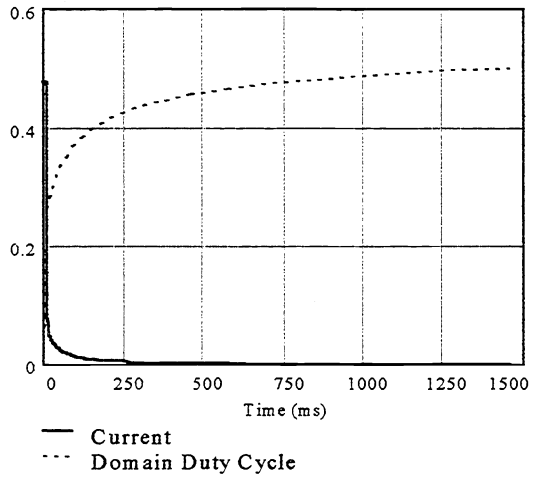

Figure 6a. Predicted poling current and domain duty cycle vs. time

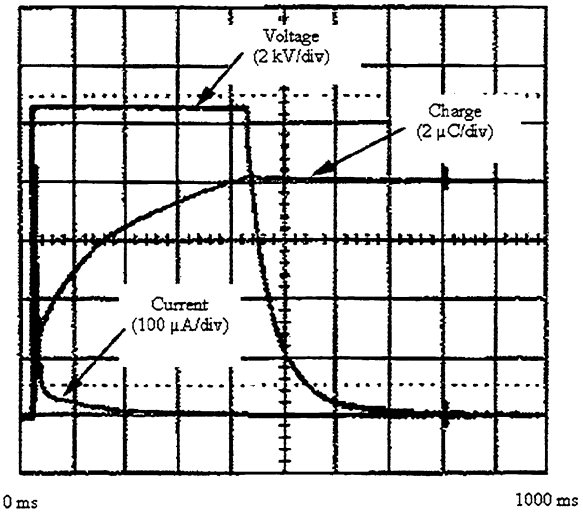

Figure 6b. Measured poling current, voltage and charge delivery vs. time.

3.5 Resulting domain pattern quality

In Figures 7a and 7b below, we show etched former +Z and +Y faces of a 500 μm thick sample poled at 20.75 kV/mm with a 6.5 μm electrode period and 1 μm wide electrolyte contact openings in a 0.5 μm thick spin-on-glass insulator. Electrolyte contact openings, rather than overcoated metal electrodes, were used to separate out effects of metallization on poling behavior. Electrostatically, electrolyte contact openings permit approximately 5% to 10% wider domains than when using overcoated electrodes, but appear to cause no significant penalty in the frequency of merged domains seen in the volume of the crystal. This sample was chosen to illustrate the domain patterning behavior we most frequently observe.

In the image of the former +Z face, note the appearance of pits along the domain-reversed stripes. Closer examination reveals that these pits are associated with bands of merged domains, such as those seen in Figure 7b. Domain merging produces fringe fields at the insulator-substrate interface of sufficient magnitude to damage the lithium niobate. When this damage occurs, the current leakage paths formed permit reduced domain pattern quality to propagate a significant distance along the electrodes.

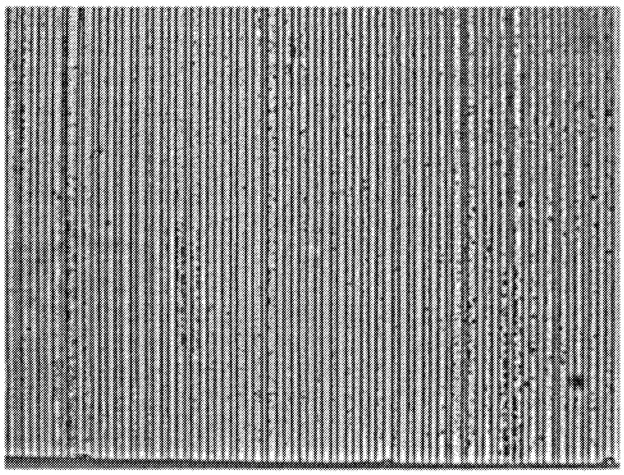

Figure 7a. 6.5 μm period, view of former +Z face. Pitted stripes are domain-reversed.

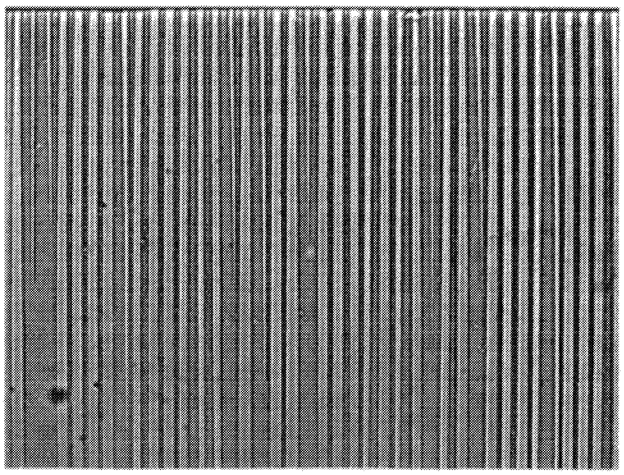

Figure 7b. 6.5 μm period, view of former +Y face near the former +Z face. Dark bands are domain-reversed.

Numerical analysis of Figure 7b indicates that the mode of the distribution of duty cycles is 31.25% (see Figure 8). In Section 3.3, the electrode width predicted to achieve a 50% domain duty cycle for overcoated electrodes was 2.7 μm. Having chosen 1 μm electrolyte contact openings for this sample, this duty cycle is consistent with expectations. There is a significant spread in duty cycle, however, and a significant contribution from merged domains (duty cycle = 100%). A plot of the percentage of merged domains vs. depth is shown in Figure 9, and indicates that domain-merging becomes significant approximately 100 μm below the surface of the crystal. The merging of domains at depths much greater than the electrode period suggests the presence of defect mechanisms within the crystal which cannot be controlled sufficiently by lithography alone.

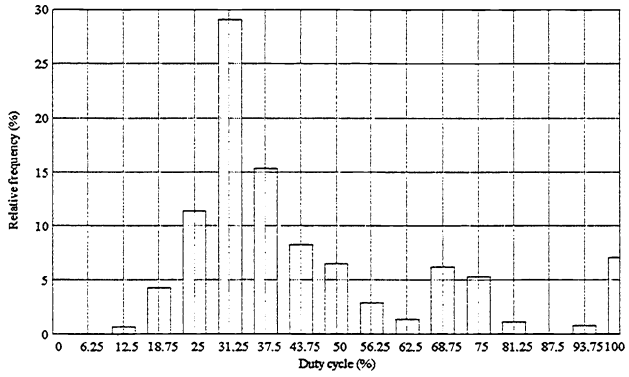

Figure 8. Histogram of domain duty cycles derived from Figure 7b.

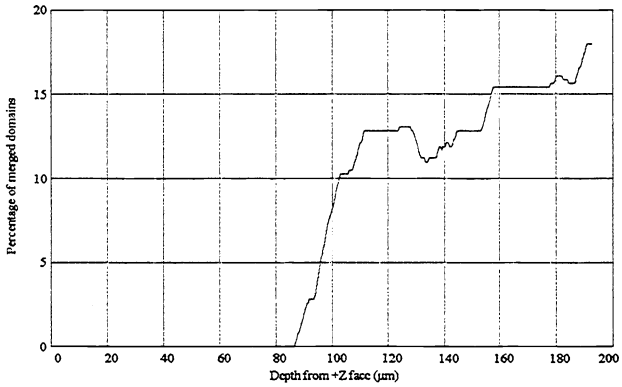

Figure 9. Percentage of merged domains as a function of depth below the patterned surface, derived from Figure 7b.

It appears from this and other samples that, apart from the influence of defect mechanisms within the substrate which can lead to domain-merging, the simple electrostatic model presented here describes the domain patterning process in lithium niobate to a significant degree. By isolating and categorizing defect mechanisms, we hope to reduce their influence in future work, as we discuss in Section 4.

4. DEFECT MECHANISMS

We have been able to identify three distinct defect mechanisms in the lithium niobate domain-patterning process. The first and most significant defect mechanism is coordinated nucleation due to sub-surface damage. The second defect mechanism is low nucleation site density. The third mechanism is the clustering of domain nucleation sites. These mechanisms and our progress in controlling them are discussed below.

4.1 Coordinated nucleation due to sub-surface damage

In Figure 7a, we saw evidence of long-range pattern degradation and associated it with domain-merging approximately 100 μm below the surface of the sample. We find that by 1% poling unpatterned full wafers, long-range paths of nucleation sites may be observed after etching. These paths appear scratch-like, but neither high optical magnification nor atomic force microscopy reveal the presence of scratches on the substrate surfaces, suggesting that sub-surface damage is involved in this unwanted nucleation. Nucleation below the surface of the crystal which is not created by the lithographically-defined electrodes will produce dielectric damage at the surface which can propagate patterning defects over long distances -- typically hundreds of microns away from the original nucleus. When unwanted nucleation sites are coordinated along scratch-like paths, the impact on process yield can be prohibitive.

We find that low-pressure lapping can significantly reduce the density of these features, consistent with the supposition that they are largely due to sub-surface lapping damage. We are currently working to identify repeatable lapping conditions and inspection techniques to routinely eliminate this source of defects.

4.2 Low nucleation site density

The model discussed in Section 3 presupposes a nucleation site density on the order of one nucleus per square period. We find, however, that when poling at the maximum contrast field, nucleation site densities are typically two to three orders of magnitude below the desired level. Low nucleation site density reduces the effective process contrast, since each isolated domain is free to spread under the insulator without significantly reducing the average substrate field in its vicinity. The scatter in points shown in Figure 3 is reduced at higher fields, suggesting that above 22 kV/mm nucleation site density is not a function of pulse length. We will be measuring nucleation site densities at elevated fields to determine whether lithium niobate is intrinsically capable of producing sufficiently high densities for repeatable patterning of visible SHG devices.

4.3 Clustered domain nucleation

We observed during the domain wall velocity measurements that domains would often nucleate in clusters. In domain-patterning experiments using samples with reduced sub-surface damage, we again observed nucleation in clusters. To investigate the influence of domain clusters on pattern quality, we poled a series of lithographically patterned samples (periods ranging from 1.75 μm to 14 μm, various electrode widths, spin-on-glass insulator, sample thicknesses of 250 μm and 500 μm) with 0.1% to 100% of the charge required for complete domain patterning. We observed that clustered nucleation followed a characteristic sequence of events:

1. An isolated domain nucleates at an electrode and propagates to the opposite crystal face.
2. The isolated domain widens along the electrode and begins to spread under the insulator.
3. Nearly simultaneously with step 2, domains nucleate around the first domain, typically nucleating on the electrode pattern. The new nuclei are typically formed within a radius of 15 μm.
4. The newly nucleated domains widen along the electrode and begin to spread under the insulator, along with the original domain.
5. New domains nucleate around the central group of domains, again within a typical zone radius of approximately 15 μm.

Steps 4 and 5 are repeated as the cluster grows. During the early stages of this process, the domains are free to spread under the insulator and merge, since they are essentially isolated domains. As the cluster grows, it forms a band of domains with a badly merged central region. We are currently investigating the origin of domain clusters and seeking methods to reduce or eliminate their density. We are also investigating the possibility of reducing their influence by increasing overall nucleation site density.

5. OPTICAL PERFORMANCE

To characterize the optical performance of samples prepared as discussed in Section 3, we polished the X-faces of a 2.4 mm long section of one sample and loosely focused the output of a single frequency Nd:YAG laser through the crystal and measured the second harmonic output power as a function of temperature. We found that the width of the temperature-tuning curve was close to that for an ideal 2.4 mm long sample, indicating that the substrate homogeneity and the long-range order of the domain pattern were not significant limiting factors to the device's conversion efficiency. The peak efficiency was only 17.4% of nominal, indicating that merged domains occupied a significant volume of the sample. In Figure 10, the measured tuning curve is shown along with a fit based on the full sample length. The normalized efficiency is defined here as the ratio of the actual efficiency to that of an ideal first-order QPM device.

We then had the sample AR-coated for use with a Q-switched Nd:YAG laser to observe behavior at high average power. The laser was focused to a 200 μm diameter spot on the endface of the crystal with up to 9 W average power incident. The Q-switched pulses were 100 ns long with an 8.4 kHz repetition rate. The crystal simultaneously produced 1.3 W of 532 nm output and 330 μW of 355 nm output at a temperature of 193°C, as shown in Figure 11. The SHG output was stable for the entire duration of the experiment.

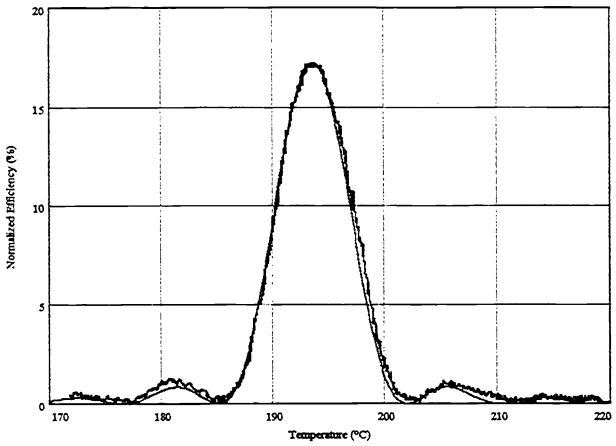

Figure 10. Temperature tuning curve for sample poled at 20.75 kV/mm with 1 μm electrodes on a 6.5 μm period, using 0.5 μm thick spin-on-glass insulator

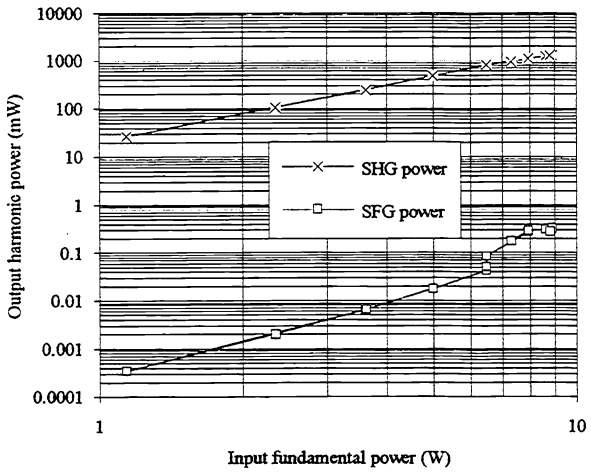

Figure 11. Average output second harmonic and sum-frequency power vs. input fundamental power.

6. CONCLUSIONS

We draw several conclusions from this work. First, a model of the wall propagation regime of domain formation in lithium niobate adequately predicts poling behavior. Second, usable domain patterns for visible light generation can be repeatably produced in 500 μm thick lithium niobate. Third, device quality appears to be limited mainly by three sources of defects: lapping-induced sub-surface damage, low nucleation site density, and clustered domain nucleation. Fourth, electric-field-poled lithium niobate can be used in high average power applications, since 1.3 W average power of 532 nm harmonic output has been stably achieved from a 9 W average power Q-switched Nd:YAG laser.

Looking forward, we anticipate that, by substantially reducing the level of defects due to sub-surface lapping damage and by increasing nucleation site density, full 3" wafers of lithium niobate will be repeatably patterned for visible light generation devices.

7. ACKNOWLEDGMENTS

We wish to thank W. Tulloch at Stanford for substantial assistance in conducting the high power laser experiments, J. Vrehl at Stanford for preparing samples for this work, D. Jundt at Crystal Technology for providing lithium niobate substrates and for many helpful discussions, and L. Myers at Wright Patterson AFB for helpful discussions throughout this research.

8. REFERENCES

[1] Fejer, M.M., et al., "Quasi-phase-matched second harmonic generation: tuning and tolerances." IEEE Journal of Quantum Electronics, (Nov. 1992) vol. 28, no. 11, p. 2631-2654.

[2] Taya,M., et al., "Modeling of Photorefractive Index Changes in Periodically-Poled Photovoltaic Media." Stanford University Center for Nonlinear Optical Materials Annual Report, August 1994-1995.

[3] Yamada, M., et al., "First-order quasi-phased matched $LiNbO_3$ waveguide periodically poled by applying an external field for efficient blue second-harmonic generation," Applied Physics Letters, vol. 62, no. 5, 1 Feb. 1993.

[4] Webjorn, J., et al. "Quasi-phase-matched blue light generation in bulk lithium niobate, electrically poled via periodic liquid electrodes." ELECTRONICS LETTERS (26 May 1994) vol. 30, no. 11, p. 894-5.

[5] Mizuuchi, K. and Yamamoto, K., "Harmonic blue light generation in bulk periodically poled $LiTaO_3$," Applied Physics Letters, vol. 66, no. 22, 29 May 1995.

[6] Chen, Q., et al. "Periodic poling of KTP using an applied electric field." ELECTRONICS LETTERS (1 Sept. 1994) vol. 30, no. 18, p. 1516-17.

[7] Baldi, P., et al. "Simultaneous generation of red, green and blue light in room temperature periodically poled lithium niobate waveguides using single source." ELECTRONICS LETTERS (3 Aug. 1995) vol. 31, no. 16, p. 1350-1.

[8] Myers, L.E., et al. "Quasi-phase-matched optical parametric oscillators in bulk periodically poled $LiNbO_3$." Journal of the Optical Society of America B (Optical Physics). (Nov. 1995). vol. 12, no. 11, p. 2102-16.

[9] Pruneri, V. et al. "Highly-efficient first-order quasi-phase-matched frequency doubling to blue of a cw diode-pumped 946 nm Nd:YAG laser." Advanced Solid State Lasers, January 31 - February 2, 1996, WB1-1.

[10] Pruneri, V. et al. "Highly-efficient second harmonic generation of green light from picosecond pulses in bulk quasi-phase-matched lithium niobate." Advanced Solid State Lasers, January 31 - February 2, 1996, FG1-1.

[11] Hayashi, M. "Kinetics of Domain Wall Motion in Ferroelectric Switching. I. General Formulation.", Journal of the Physical Society of Japan. (Sept. 1972). vol. 33, no. 3, p. 616-628.